366
Copy
RM E53J27

NACA RM E53J27

NACA

RESEARCH MEMORANDUM

AERODYNAMICS OF SLENDER BODIES AT MACH NUMBER OF 3.12 AND REYNOLDS NUMBERS FROM 2×10^6 TO 15×10^6

IV - AERODYNAMIC CHARACTERISTICS OF SERIES OF FOUR BODIES HAVING NEAR-PARABOLIC NOSES AND CYLINDRICAL AFTERBODIES

By John R. Jack and Barry Moskowitz

Lewis Flight Propulsion Laboratory
Cleveland, Ohio

NATIONAL ADVISORY COMMITTEE FOR AERONAUTICS

WASHINGTON

January 25, 1954

3036

CU-1

NATIONAL ADVISORY COMMITTEE FOR AERONAUTICS

RESEARCH MEMORANDUM

AERODYNAMICS OF SLENDER BODIES AT MACH NUMBER OF 3.12 AND REYNOLDS NUMBERS FROM 2×10^6 TO 15×10^6. IV - AERODYNAMIC CHARACTERISTICS OF SERIES OF FOUR BODIES HAVING NEAR-PARABOLIC NOSES AND CYLINDRICAL AFTERBODIES

By John R. Jack and Barry Moskowitz

SUMMARY

Pressure distributions and forces have been obtained for a series of four bodies of revolution with nose-fineness ratios varying from 4 to 10. This experimental investigation was conducted in the NACA Lewis 1- by 1-foot supersonic wind tunnel at a Mach number of 3.12 for a Reynolds number range of 2×10^6 to 14×10^6 (based on model length) and for an angle-of-attack range from zero to 9°.

Pressure distributions on a representative model for the small angles of attack were adequately predicted by a hybrid theory which is composed of a first-order crossflow solution plus a second-order axial-flow solution. At the larger angles of attack, the agreement was fair except in the region where the effects of crossflow separation predominated, for which case the agreement was poor. A large change in the base pressure coefficient of the representative model occurred between the Reynolds numbers of 2×10^6 and 8×10^6; no further change took place as the Reynolds number increased to 14×10^6.

The total drag coefficients for small angles of attack at Reynolds numbers of 8×10^6 and 14×10^6 were approximately equal and slightly higher than the drag coefficient for 2×10^6. A comparison of the experimentally determined lift and moment coefficients with the hybrid theory plus the viscous crossflow force showed good agreement at all Reynolds numbers and angles of attack investigated. The force coefficients decreased with an increase in nose-fineness ratio. The forebody lift-drag ratio increased with both angle of attack and nose-fineness ratio in the range investigated.

INTRODUCTION

As part of a systematic program to ascertain the effects of Reynolds number on aerodynamic characteristics, to extend the basic information on the aerodynamics of bodies of revolution, and to assess the validity of several theories for predicting pressures and forces acting on bodies, tests are being conducted in the NACA Lewis 1- by 1-foot supersonic wind tunnel on a series of bodies of revolution. The first three parts of this series of investigations are reported in references 1 to 3. Reference 1 reported the complete aerodynamic characteristics of a near-parabolic nose body, while reference 2 reported the load distributions of a series of five bodies having conical or slightly blunted noses and cylindrical afterbodies. The boundary-layer development and the forces acting on a typical cone-cylinder body of revolution were reported in reference 3. The subject of the present report is the aerodynamic characteristics of a series of four bodies having near-parabolic noses and cylindrical afterbodies at a Mach number of 3.12 for Reynolds numbers from 2×10^6 to 14×10^6 (based on model length) and angles of attack from zero to 9°. The over-all fineness ratio of the four bodies was 12, while the nose-fineness ratio varied from 4 to 10.

Pressure distributions were obtained for all models at a Reynolds number of 14×10^6 and at Reynolds numbers of 2×10^6 and 8×10^6 for a representative model. Forces were obtained for all models over the Reynolds number range. The experimentally determined pressure distributions for the representative model were compared with a second-order theory for zero angle of attack and a hybrid theory for angle of attack. The forces were compared with the preceding theories plus a viscous crossflow theory at angle of attack.

SYMBOLS

The following symbols are used in this report:

A_F	frontal area
C_D	drag coefficient, $D/q_0 A_F$
C_L	lift coefficient, $L/q_0 A_F$
C_M	pitching-moment coefficient about base of model, $M/q_0 A_F l$
C_p	pressure coefficient, $\frac{p-p_0}{q_0}$
D	drag force

3036

d	body diameter
L	lift force
l	length of model
l_n	length of model nose
M	pitching moment
p	static pressure
q_0	free-stream dynamic pressure, $1/2\rho_0 U_0^2$
R	maximum body radius
Re	Reynolds number, $\rho_0 U_0 l/\mu$
U_0	free-stream velocity
x,r,θ	cylindrical coordinates
α	angle of attack, deg
γ	ratio of specific heats, 1.40
μ	kinematic viscosity
ρ_0	free-stream density

Subscripts:

b	base
α	due to angle of attack
0	free-stream conditions

APPARATUS AND PROCEDURE

Wind Tunnel

The investigation was conducted in the NACA Lewis 1- by 1-foot supersonic wind tunnel, which is a nonreturn, continuous-flow, variable-pressure tunnel operating at a Mach number of 3.12. Inlet pressures may be varied from 6 to 52 pounds per square inch absolute at a stagnation temperature of approximately 60° F. The specific humidity of the air supplied to the tunnel was maintained at approximately 2×10^{-5} of a pound of water per pound of dry air, which minimized the effects of condensation. The free-stream Reynolds number has a range of approximately 1×10^6 to 8×10^6 per foot.

3036

Models

Sketches of the models investigated, with pertinent dimensions, are presented in figure 1. The defining equation for the nose of each body is

$$\frac{r}{R} = \left[2\frac{x}{l_n} - \left(\frac{x}{l_n}\right)^2\right]^{3/4} \qquad (1)$$

Although equation (1) predicts an infinite slope at the tip of the bodies, for all practical purposes the models, when machined, had pointed noses. The nose-fineness ratios of the bodies are 4, 6, 8, and 10, and the overall fineness ratio is 12. Pressure-distribution models were machined from steel, while force models were made from aluminum. All models were polished to a 16-microinch finish. Each model was sting supported from the rear (fig. 2).

Measurements

Axial pressure distributions for the bodies of revolution were determined from two rows of static-pressure orifices placed 90° apart. Meridional pressure distributions were obtained for selected axial stations through orifices placed 22.5° apart. To keep the amount of instrumentation to a minimum, the models were instrumented in one quadrant only and then tested at both positive and negative angles of attack so that pressure distributions would be complete with respect to the meridian angle. Base pressures were determined from four static-pressure orifices, placed 30° apart and located in one quadrant.

Forces were measured by a three-component strain-gage balance, which was attached to a sting-strut combination. A static calibration of the balance showed an interaction between the normal and axial forces; therefore, corrections for this interaction were made in the reduction of the force data. The maximum experimental errors in the force coefficients are believed to be as follows for the lowest and highest Reynolds numbers, respectively:

Force coefficient	Maximum error at Reynolds number	
	2×10^6	14×10^6
C_D	±0.01	±0.002
C_L	$\pm.02$	$\pm.002$
C_M	$\pm.002$	$\pm.001$

3036

Reduction of Data and Methods of Computation

The free-stream static pressure used in reducing the experimental data to coefficient form is that obtained from the side wall of the tunnel opposite the model vertex. This pressure was in close agreement with the static pressure measured on the center line of the tunnel at the same axial station. Incremental pressure coefficients due to angle of attack were obtained by subtracting the measured values at zero angle of attack from those measured at angle of attack.

The second-order theory of reference 4 as applied in reference 5 was used to obtain theoretical pressure distributions. Although the theory, as developed in reference 4, is strictly applicable for sharp-nosed bodies of revolution at Mach numbers less than that for which the Mach cone surface coincides with the model tip surface, it has been applied in the present case by replacing the blunt tip given by equation (1) with a short conical section. The conical section was chosen such that the cone half angle was less than 94 percent of the Mach angle in order to utilize the tables presented in reference 5. The conical section was approximately 2 percent of the body length.

For angle of attack, theoretical pressure distributions were calculated by using the hybrid theory suggested in reference 4 and were applied in the same manner as that given in reference 3. The hybrid theory consists of the second-order axial-flow solution of reference 4 combined with a first-order crossflow solution of reference 6. The theoretical forces, for angle of attack, were computed by using the integrated hybrid-theory pressure distributions plus the viscous cross-force theory of reference 7.

RESULTS AND DISCUSSION

The experimental results consist of pressure distributions and forces for the models presented in figure 1 and for angles of attack from zero to 9°. The pressure-distribution results are discussed for all models at zero angle of attack; however, because the effects of angle of attack do not vary significantly with the models, these effects are discussed only for model 2, which has a nose-fineness ratio of 6.[1]

Pressure Distributions. - At zero angle of attack, the experimental variation of the pressure coefficient with axial station for all models at a Reynolds number of 14×10^6 is presented in figure 3. As expected, the level of the nose pressure distributions increased with decreasing nose-fineness ratio; consequently, the wave drag will have the same trend.

Figure 4 shows the variation of the axial pressure distribution of model 2 at zero angle of attack for the three Reynolds numbers investigated. Compared with the experimental data of figure 4 is the pressure distribution obtained from the second-order theory of reference 4. The agreement between the second-order theory and experiment is good, with the best agreement at Reynolds numbers of 8×10^6 and 14×10^6. An integration of the pressure distributions of figure 4 reveals that the effect of Reynolds number on the wave drag is very small.

The incremental axial pressure distributions due to angle of attack for three Reynolds numbers are presented in figures 5 and 6 for the bottom (meridian angle of 0°) and top (meridian angle of 180°), respectively, of the representative model. In general, an increase in Reynolds number from 2×10^6 to 8×10^6 causes an increase in the incremental pressure-distribution level. Angle-of-attack data for models 1, 3, and 4 are given in tables I, II, and III, respectively, for a Reynolds number of 14×10^6.

Increments in pressure coefficient due to angle of attack for model 2 are compared in figures 5 and 6 with the hybrid theory of reference 4. Agreement between experiment and theory is quite good at an angle of attack of 3°; however, at angle of attack of 9°, the agreement is poor in several regions on the body. At the tip of the model for a meridian angle of zero, the poor agreement is due to an inadequacy in the hybrid theory at high angles of attack. For the conical tip used in the calculation, the pressure coefficient obtained from hybrid theory is about 20 percent higher than that obtained from cone theory (ref. 8). On the cylindrical portion of the model, the disagreement for a meridian angle θ of 180° (fig. 6) is due to

[1]A detailed analysis of the aerodynamic characteristics of model 2 including the boundary-layer development, friction drags, and transition studies has been reported previously in reference 1. For completeness, this model was retested with the present series.

3036

crossflow separation; while for a meridian angle of zero (fig. 5), the difference between theory and experiment in the region $x = 11$ to 17 inches appears to be due to a small local tunnel disturbance. It is not known, however, why this discrepancy is much more pronounced at an angle of attack of 9° than at an angle of attack of 3°. It is possible that an interaction of the disturbance with the separated crossflow is involved. At an angle of attack of 3°, the crossflow separates near the top of the body ($\theta = 180^{\circ}$); while at an angle of attack of 9°, crossflow separation has moved to $\theta = 90^{\circ}$. A local increase in effective cross section due to increased crossflow separation could influence pressures at the bottom of the body in the observed manner.

Plotted in figure 7 is the experimental variation of the incremental pressure coefficient due to angle of attack with meridional angle for three axial stations, the first of which is on the nose of the model while the other two are on the cylindrical afterbody. Agreement between experiment and theory is good at an angle of attack of 3°, and again the agreement at an angle of 9° is poor for the reasons mentioned in the discussion of figures 5 and 6. The effect of crossflow separation is readily shown in figure 7. At the forward stations, the agreement between theory and experiment is good on the leeward side of the body; while, for the axial stations located on the cylinder, large disagreement between theory and experiment is noted in the same region because the crossflow has separated. The separation occurred at $\theta = 110^{\circ}$ for the 14-inch station and at $\theta = 50^{\circ}$ for the 20.5-inch station.

The effect of Reynolds number upon the base pressure of model 2 is presented in figure 8(a). A large change in the base pressure occurred between the Reynolds numbers of 2×10^{6} and 8×10^{6}, with no further change as the Reynolds number increased to 14×10^{6}. As the Reynolds number increased from 2×10^{6} to 8×10^{6}, the transition point moved from the base of the model to a point approximately 12 inches upstream of the model base (ref. 1). Figure 8(b) illustrates that the base pressure is relatively insensitive to nose-fineness ratio for a Reynolds number of 14×10^{6} and for the angle-of-attack range investigated. Almost all the base pressure coefficients are within ±2 percent of a median curve drawn through the experimental data.

Forces. - The variation of total-drag coefficient with angle of attack for all models is given in figure 9 for nominal Reynolds numbers of 2×10^{6}, 8×10^{6}, and 14×10^{6}. At angles of attack of zero and 3°, the drag coefficients at 8×10^{6} and 14×10^{6} are approximately equal and slightly higher than the drag coefficient for 2×10^{6}. This Reynolds number effect at the lower angles of attack is attributed to an increase in friction drag and base drag due to a forward movement of transition with increasing Reynolds number, since as noted previously the pressure drag is essentially invariant with an increasing Reynolds number.

Experimentally determined lift coefficients for all four models are presented in figure 10. Compared with the data for the representative model is the hybrid theory of reference 4 plus the viscous crossflow force theory of reference 7. The agreement between theory and experiment is good for the angle-of-attack and Reynolds number range investigated. The lift coefficient is little affected by the variation in Reynolds number.

Pitching-moment coefficients about the bases of the models and centers of pressures are given in figures 11 and 12, respectively. As in the case of the lift coefficient, the pitching moment and center of pressure are not greatly influenced by a varying Reynolds number. A comparison of theory and experiment again shows good agreement and a prediction of the proper trends. 3036

To summarize the effect of nose-fineness ratio, all the force parameters investigated, including the forebody lift-drag ratio, have been plotted against nose-fineness ratio for a Reynolds number of 14×10^6 (fig. 13). The force parameters decreased with increasing nose-fineness ratio except for the lift-drag ratio of the forebody (body forward of the base), which increased. At the higher angles of attack, the forebody lift-drag ratio appears to have reached a maximum at a nose-fineness ratio of 10.

SUMMARY OF RESULTS

The aerodynamic characteristics of four bodies of revolution having nearly parabolic noses with fineness ratios varying from 4 to 10 have been investigated in the NACA Lewis 1- by 1-foot variable Reynolds number tunnel at a Mach number of 3.12. An analysis of the results has led to the following conclusions:

1. The base pressure and the zero angle-of-attack pressure-distribution level decreased with an increase in the Reynolds number from 2×10^6 to 8×10^6; however, the incremental pressure distribution due to angle of attack and the total-drag coefficient for zero and 3° angles of attack increased in this range. No Reynolds number effects were noted for an increase from 8×10^6 to 14×10^6.

2. The level of the nose pressure distributions increased with decreasing nose-fineness ratio. However, the base pressures for a Reynolds number of 14×10^6 were little affected by a change in nose-fineness ratio for the angle-of-attack range investigated. In general, the respective force coefficients decreased with an increase in nose-fineness ratio. The forebody lift-drag ratio increased with both nose-fineness ratio and angle of attack.

3. The second-order theory of Van Dyke adequately predicted the zero angle-of-attack pressure distribution for the representative model. A combination of the second-order axial-flow solution with the first-order crossflow solution predicted the incremental pressure distributions due to angle of attack well, except on the tip of the model (meridian angle of zero) and in the regions of separated crossflow. The measured force coefficients were estimated closely by integrating the pressure distributions obtained from the hybrid theory and adding to this force the viscous crossflow force.

3036

Lewis Flight Propulsion Laboratory
National Advisory Committee for Aeronautics
Cleveland, Ohio, November 10, 1953

CU-2

REFERENCES

1. Jack, John R., and Burgess, Warren C.: Aerodynamics of Slender Bodies at Mach Number of 3.12 and Reynolds Number from 2×10^6 to 15×10^6. I - Body of Revolution with Near-Parabolic Forebody and Cylindrical Afterbody. NACA RM E51H13, 1951.

2. Jack, John R., and Gould, Lawrence I.: Aerodynamics of Slender Bodies at Mach Number of 3.12 and Reynolds Number from 2×10^6 to 15×10^6. II - Aerodynamic Load Distributions of Series of Five Bodies Having Conical Noses and Cylindrical Afterbodies. NACA RM E52C10, 1952.

3. Jack, John R.: Aerodynamics of Slender Bodies at Mach Number of 3.12 and Reynolds Number from 2×10^6 to 15×10^6. III - Boundary Layer and Force Measurements on Slender Cone-Cylinder Body of Revolution. NACA RM E53B03, 1953.

4. Van Dyke, Milton D.: First- and Second-Order Theory of Supersonic Flow Past Bodies of Revolution. Jour. Aero. Sci., vol. 18, no. 3, Mar. 1951, pp. 161-178.

5. Van Dyke, Milton D.: Practical Calculation of Second- Order Supersonic Flow Past Nonlifting Bodies of Revolution. NACA TN 2744, 1952.

6. Tsien, Hsue-Shen: Supersonic Flow Over an Inclined Body of Revolution. Jour. Aero. Sci., vol. 5, no. 12, Oct. 1938, pp. 480-483.

7. Allen, H. Julian: Estimation of the Forces and Moments Acting on Inclined Bodies of Revolution of High Fineness Ratios. NACA RM A9I26, 1949.

8. Anon.: Tables of Supersonic Flow Around Cones of Large Yaw. Tech. Rep. No. 5, Dept. Elec. Eng., M.I.T., 1949.

TABLE I. - PRESSURE COEFFICIENTS FOR MODEL 1 FOR TWO ANGLES OF ATTACK AND REYNOLDS NUMBER OF 14×10^6

(a) Axial variation of pressure coefficient.

Angle of attack, $\alpha = 3^\circ$

Axial station, x, in.	Meridian angle, θ, deg	
	0	180
1	-----	0.074
2	0.104	.033
3	.064	.010
4	.041	-.004
5	.021	-.015
5.5	.016	-.019
6	.004	-.020
6.5	-.002	-.023
7	-.007	-.026
7.5	-.008	-.023
8	-.007	-.020
8.5	-.006	-.017
9	-.004	-.014
11	-.003	-.011
13	-.006	-.008
15	-.007	-.008
17	-.008	-.002
19	-.003	-.007
20.5	-.006	-.008

Angle of attack, $\alpha = 9^\circ$

Axial station, x, in.	Meridian angle, θ, deg	
	0	180
1	-----	0.022
2	0.196	-.005
3	.152	-.016
4	.120	-.024
5	.087	-.030
5.5	.075	-.033
6	.064	-.035
6.5	.053	-.036
7	.043	-.035
7.5	.040	-.034
8	.039	-.030
8.5	.039	-.026
9	.038	-.022
11	.035	-.018
13	.034	-.014
15	.032	-.017
17	.022	-.020
19	.026	-.031
20.5	.023	-.031

(b) Circumferential variation of pressure coefficient.

Angle of attack, $\alpha = 3^\circ$

Axial station, x, in.	Meridian angle, θ, deg						
	22.5	45	67.5	90	112.5	135	157.5
2	0.108	0.102	0.087	0.072	0.054	0.045	0.038
4	.042	.036	.031	.021	.009	.002	.001
7	-.007	-.018	-.010	-.023	-.028	-.029	-.028
11	-.003	-.008	-.014	-.018	-.018	-.014	-.012
15	-.007	-.008	-.011	-.011	-.010	-.010	-.010
20.5	-.004	-.010	-.014	-.016	-.013	-.011	-.010

Angle of attack, $\alpha = 9^\circ$

Axial station, x, in.	Meridian angle, θ, deg						
	22.5	45	67.5	90	112.5	135	157.5
2	0.185	0.148	0.098	0.047	0.012	0.010	-0.006
4	.114	.083	.038	-.005	-.034	-.036	-.027
7	.036	-.022	-.012	-.053	-.055	-.073	-.042
11	.027	.000	-.036	-.072	-.055	-.048	-.050
15	.025	-.001	-.041	-.062	-.038	-.044	-.064
20.5	.018	-.014	-.052	-.044	-.034	-.034	-.039

CONFIDENTIAL

TABLE II. - PRESSURE COEFFICIENTS FOR MODEL 3 FOR TWO ANGLES OF ATTACK AND REYNOLDS NUMBER OF 14×10^6

(a) Axial variation of pressure coefficient.

Angle of attack, $\alpha = 3^\circ$		
Axial station, x, in.	Meridian angle, θ, deg	
	0	180
2	0.065	0.013
3	.047	.005
4	.040	.004
5	.031	-.002
6	.026	-.002
7	.021	-.002
8	.016	-.004
9	.012	-.005
10	.008	-.008
11	.004	-.012
12	.000	-.014
12.5	-.002	-.015
13	-.006	-.016
13.5	-.007	-.016
14	-.008	-.015
14.5	-.008	-.016
15	-.007	-.015
15.5	-.009	-.014
17	-.008	-.009
18.75	-.008	-.012
20.5	-.009	-.012

Angle of attack, $\alpha = 9^\circ$		
Axial station, x, in.	Meridian angle, θ, deg	
	0	180
2	0.104	-0.006
3	.094	-.012
4	.091	-.014
5	.087	-.016
6	.080	-.017
7	.074	-.018
8	.065	-.019
9	.062	-.020
10	.057	-.022
11	.055	-.023
12	.051	-.027
12.5	.049	-.027
13	.048	-.029
13.5	.048	-.030
14	.044	-.029
14.5	.044	-.029
15	.042	-.028
15.5	.041	-.028
17	.031	-.024
18.75	.030	-.031
20.5	.032	-.028

(b) Circumferential variation of pressure coefficient.

Angle of attack, $\alpha = 3^\circ$							
Axial station, x, in.	Meridian angle, θ, deg						
	22.5	45	67.5	90	112.5	135	157.5
3	0.048	0.046	0.037	0.027	0.014	0.009	0.006
7	.021	.018	.010	.002	-.004	-.003	-.003
11	.005	-.004	-----	-.010	-.014	-.014	-.012
14	-.006	-.008	-.012	-.017	-.019	-.018	-.015
17	-.006	-.009	-.013	-.018	-.020	-.016	-.021
20.5	-.007	-.011	-.017	-.019	-.018	-.014	-.013

Angle of attack, $\alpha = 9^\circ$							
Axial station, x, in.	Meridian angle, θ, deg						
	22.5	45	67.5	90	112.5	135	157.5
3	0.107	0.075	0.031	-0.012	-0.033	-0.032	-0.017
7	.070	.042	.001	-.037	-.054	-.033	-.025
11	.040	-.025	-----	-.060	-.040	-.058	-.041
14	.026	-.001	-.036	-.070	-.049	-.043	-.048
17	.018	-.005	-.043	-.068	-.043	-.041	-.046
20.5	.014	-.014	-.053	-.051	-.038	-.040	-.047

TABLE III. - PRESSURE COEFFICIENTS FOR MODEL 4 FOR TWO ANGLES OF ATTACK AND REYNOLDS NUMBER OF 14×10^6

(a) Axial variation of pressure coefficient.

Axial station, x, in.	Angle of attack, $\alpha = 3^{\circ}$; Meridian angle, θ, deg: 0	180
2	0.052	0.007
3	.039	.003
4	.036	.003
5	.030	.001
6	.025	-.002
7	.023	.001
8	.018	-.002
9	.015	-.001
10	.014	-.004
11	.011	-.007
12	.007	-.009
13	.002	-.011
14	.000	-.011
15	-.002	-.013
16	-.005	-.012
16.5	-.009	-.012
17	-.009	-.011
17.5	-.006	-.010
18.1	-.007	-.011
18.8	-.007	-.012
19.5	-.005	-.013
20.5	-.009	-.011

Axial station, x, in.	Angle of attack, $\alpha = 9^{\circ}$; Meridian angle, θ, deg: 0	180
2	-----	-0.008
3	0.106	-.015
4	.102	-.014
5	.096	-.015
6	.087	-.017
7	.080	-.016
8	.073	-.017
9	.068	-.020
10	.063	-.022
11	.059	-.023
12	.055	-.026
13	.050	-.029
14	.046	-.029
15	.041	-.029
16	.036	-.030
16.5	.029	-.032
17	.025	-.031
17.5	.027	-.030
18.1	.028	-.031
18.8	.025	-.035
19.5	.029	-.033
20.5	.026	-.032

(b) Circumferential variation of pressure coefficient.

Axial station, x, in.	Angle of attack, $\alpha = 3^{\circ}$; Meridian angle, θ, deg: 22.5	45	67.5	90	112.5	135	157.5
3	0.042	0.036	0.030	0.021	0.012	0.004	0.006
8	.019	.014	.005	-.002	-.004	-.004	-.003
13	.003	-.003	.000	-.009	-.013	-.011	-.012
17.5	-.005	-.011	-.015	-.019	-.021	-.017	-.013
20.5	-.007	-.012	-.017	-.020	-.018	-.015	-.013

Axial station, x, in.	Angle of attack, $\alpha = 9^{\circ}$; Meridian angle, θ, deg: 22.5	45	67.5	90	112.5	135	157.5
3	0.099	0.063	0.021	-0.014	-0.040	-0.036	-0.018
8	.065	.036	-.006	-.043	-.058	-.034	-.024
13	.042	-.027	.010	-.061	-.040	-.048	-.043
17.5	.022	-.006	-.043	-.068	-.046	-.041	-.042
20.5	.017	-.013	-.051	-.061	-.041	-.041	-.043

3036

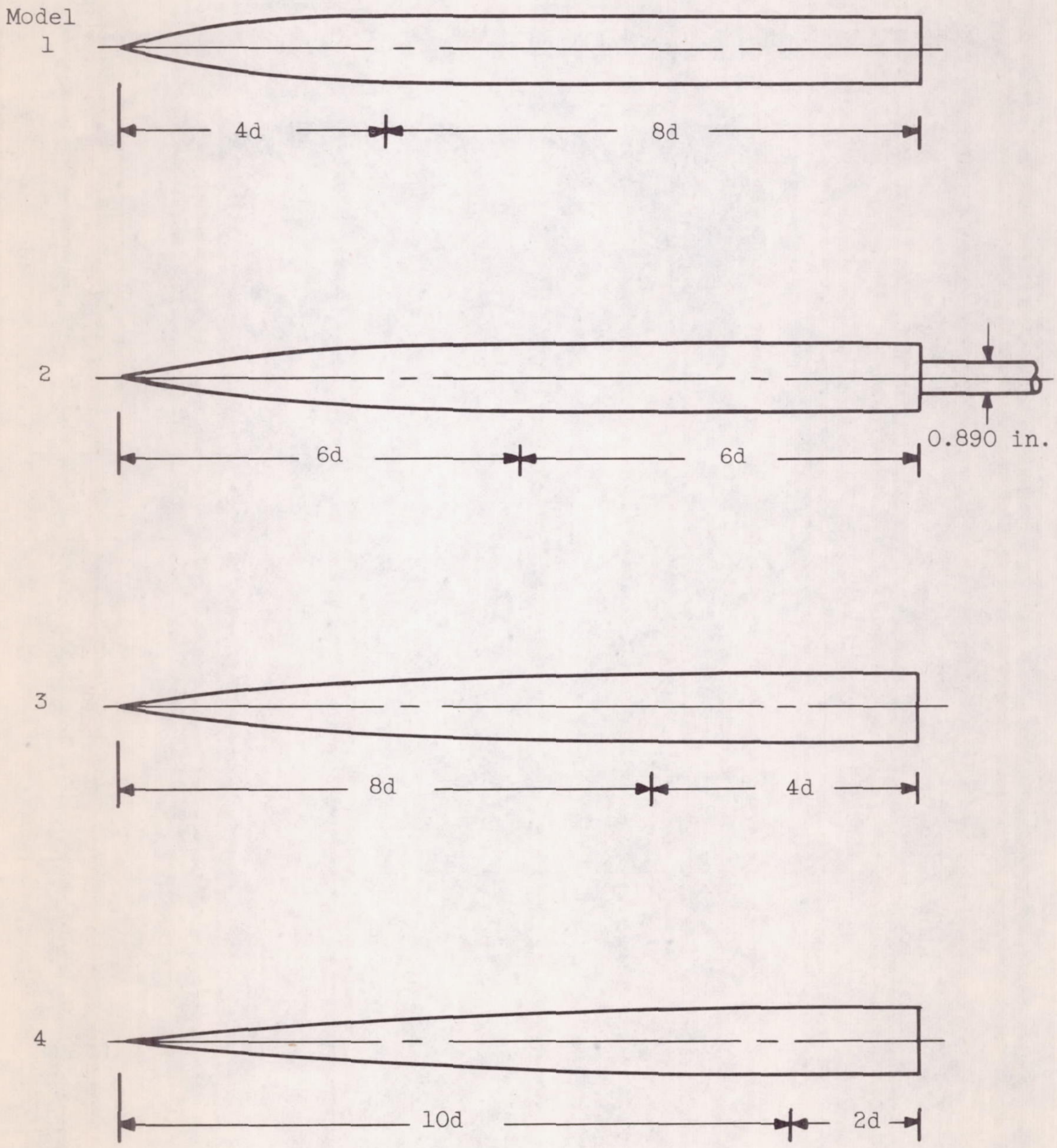

Figure 1. - Schematic drawing of models. Maximum body diameter, d, 1.75 inches.

CONFIDENTIAL

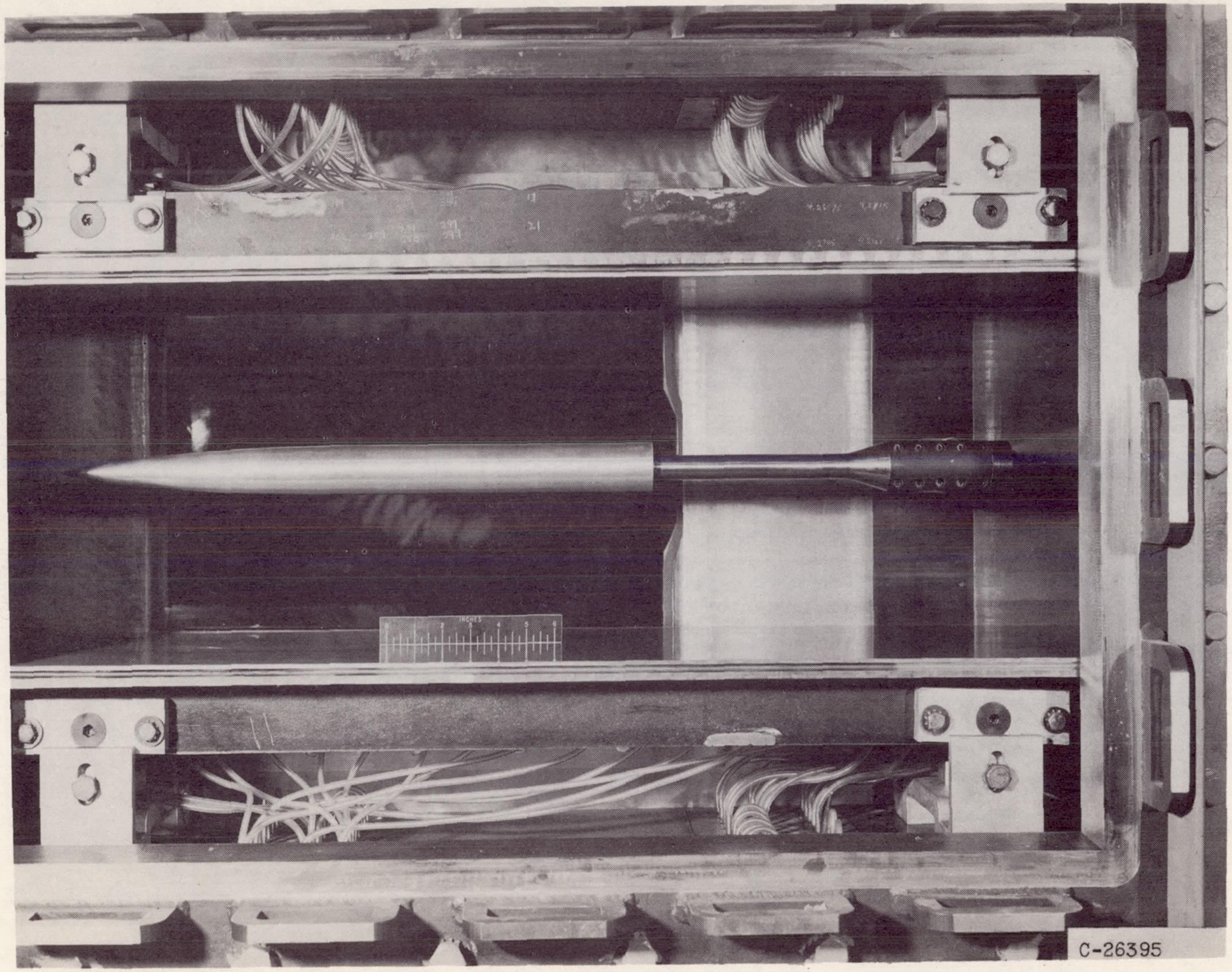

Figure 2. - Representative model 2 installed in Lewis 1- by 1-foot supersonic wind tunnel.

CONFIDENTIAL

3036

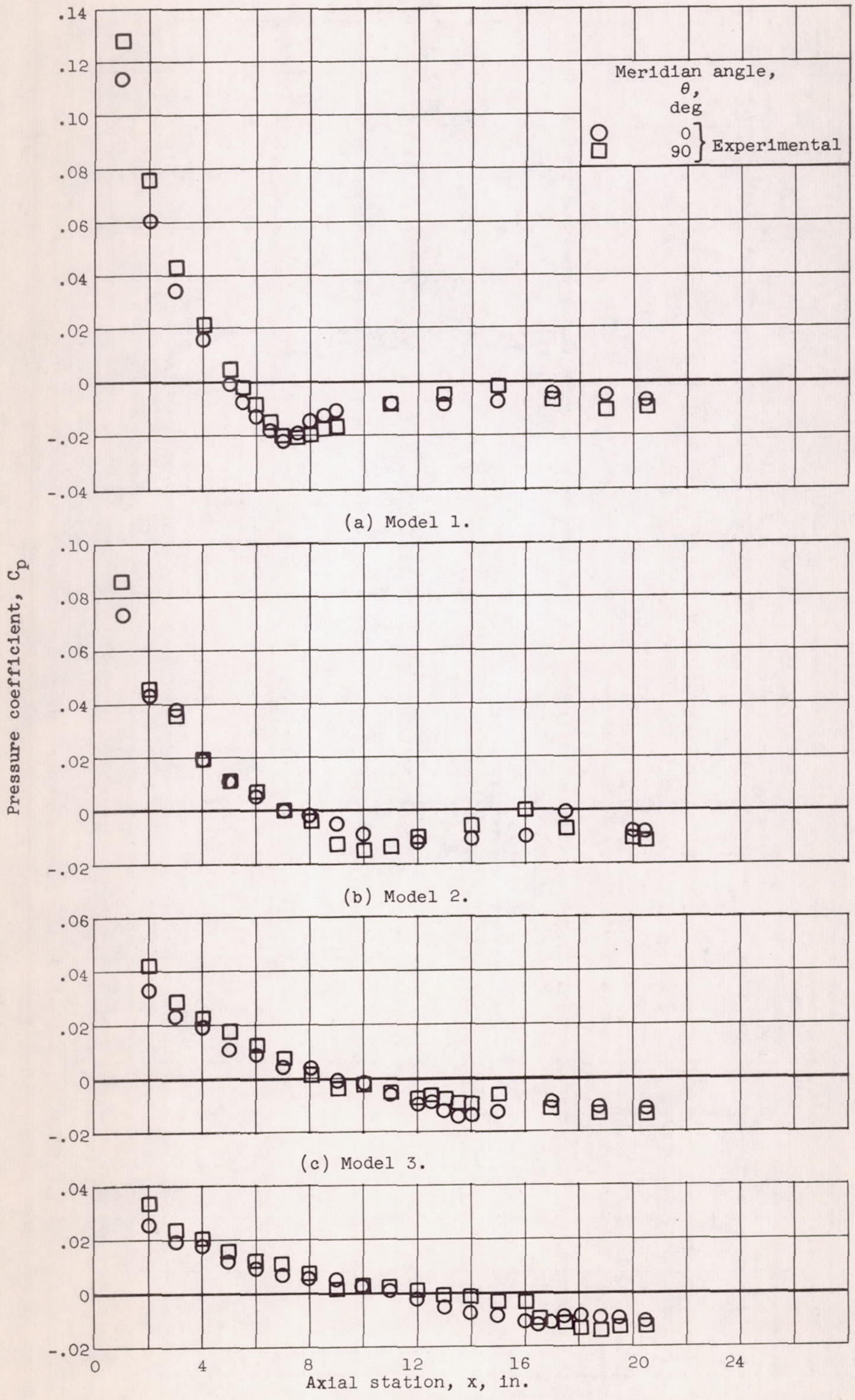

Figure 3. - Experimental axial variation of pressure coefficient for all models at zero angle of attack and Reynolds number of 14×10^6.

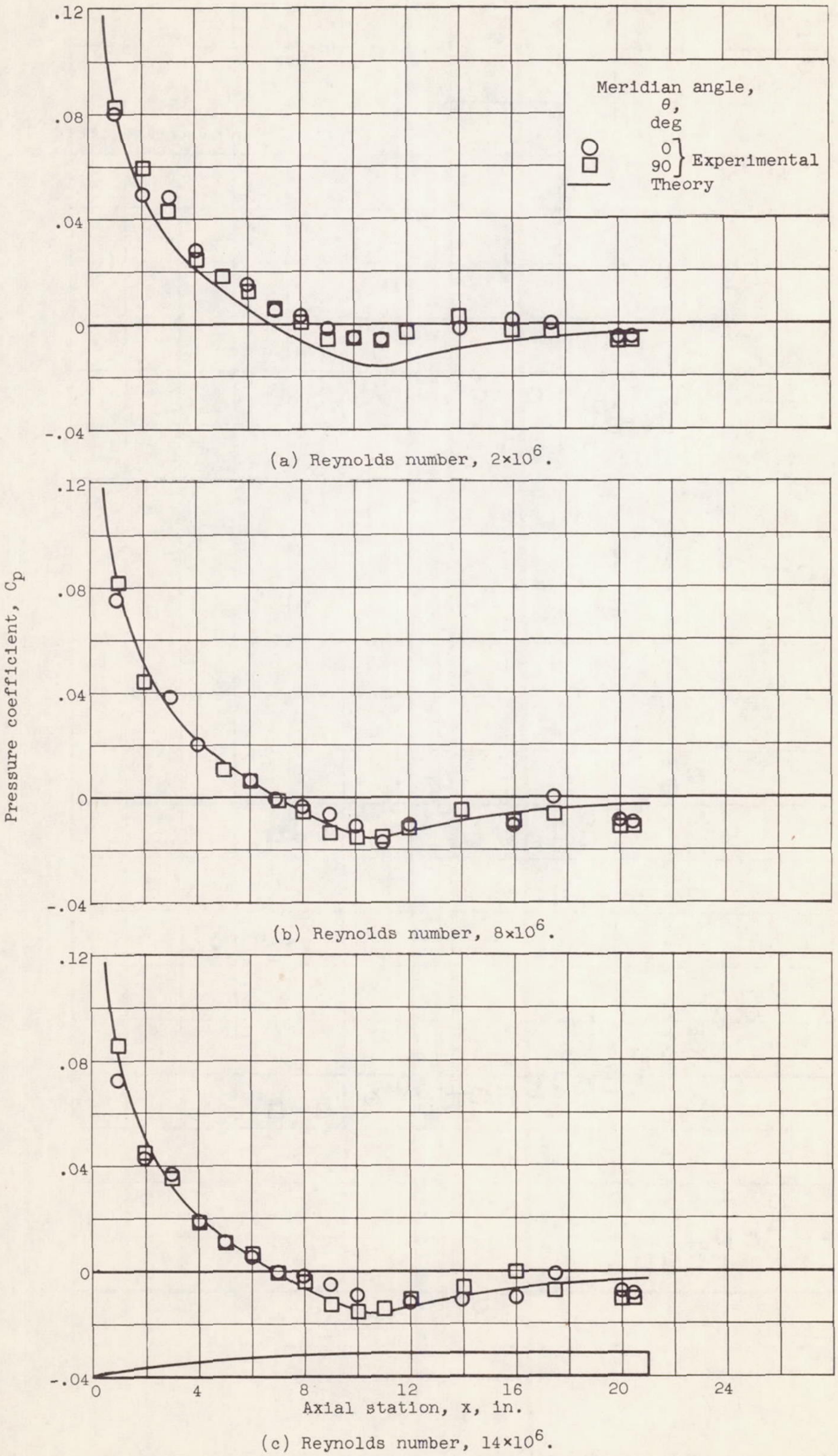

Figure 4. - Effect of Reynolds number on pressure distribution for model 2 at zero angle of attack.

3036

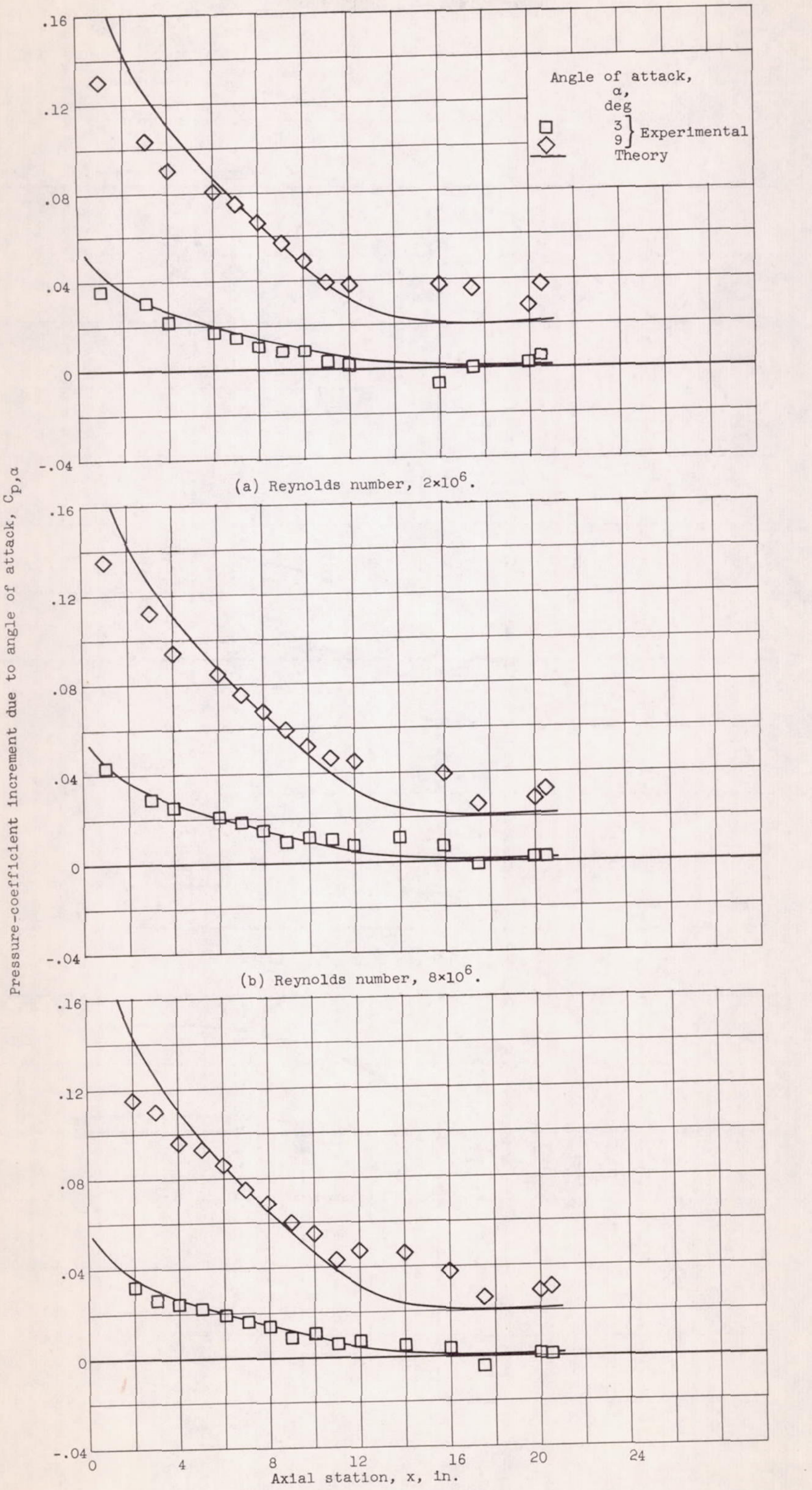

Figure 5. - Effect of Reynolds number on bottom-surface pressure distribution of model for two angles of attack. Meridian angle, 0°.

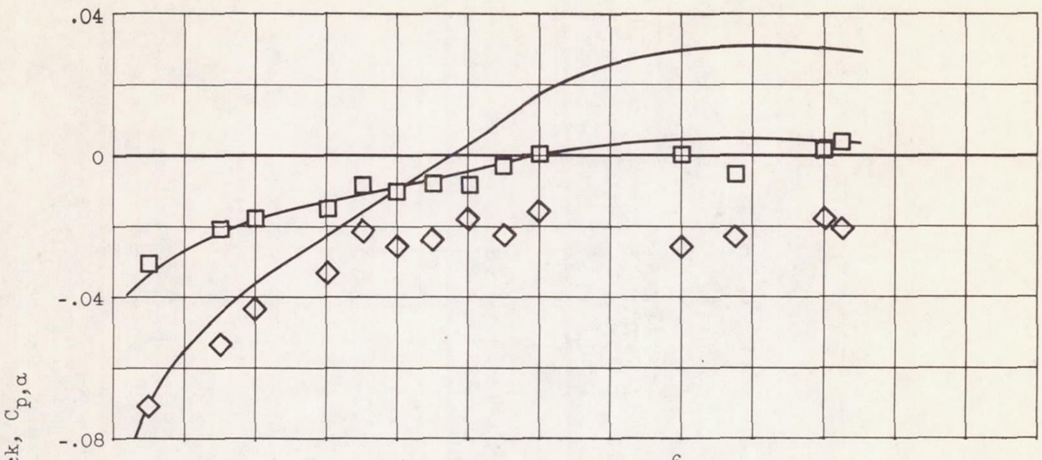

(a) Reynolds number, 2×10^6.

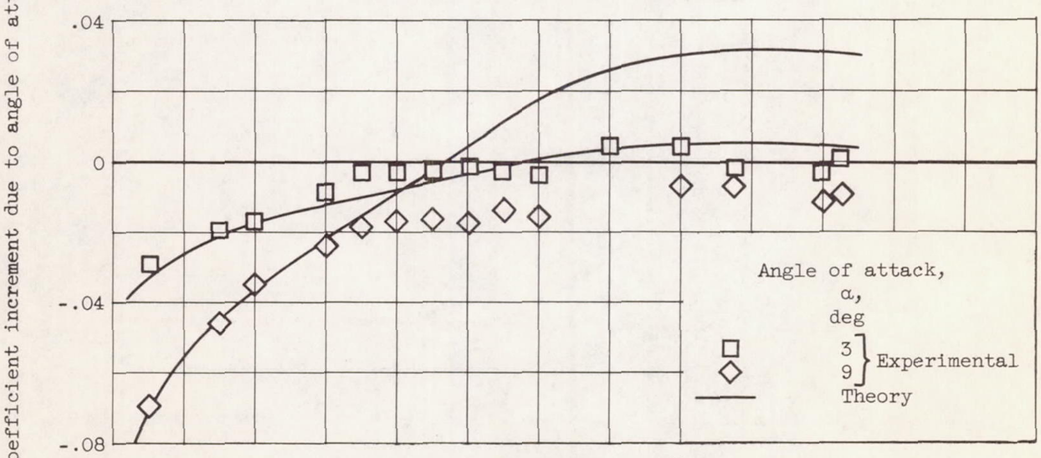

(b) Reynolds number, 8×10^6.

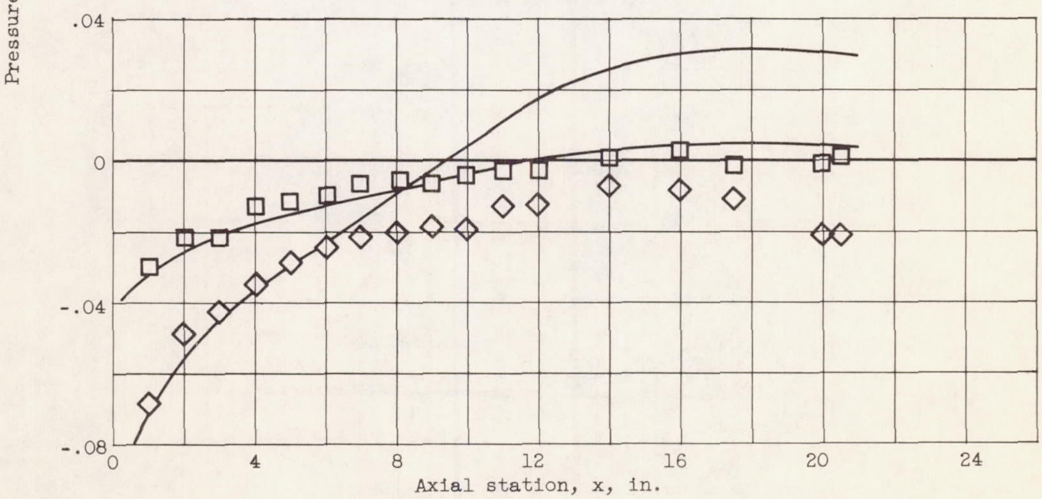

(c) Reynolds number, 14×10^6.

Figure 6. - Effect of Reynolds number on the top-surface pressure distribution of model 2 for two angles of attack. Meridian angle, 180°.

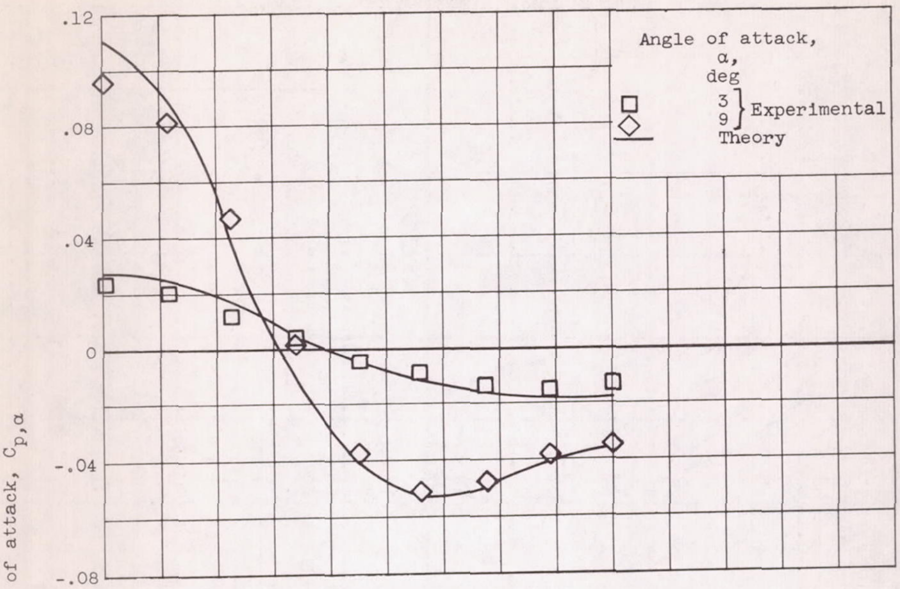

(a) Axial station, 4 inches.

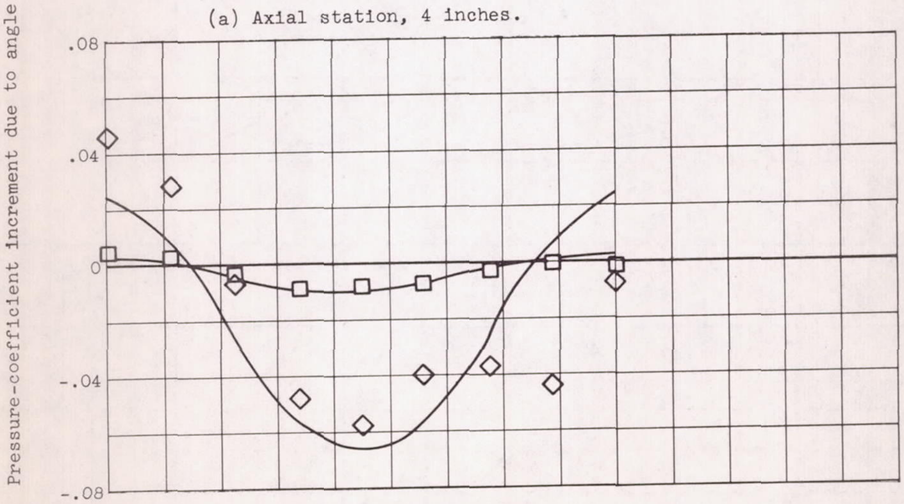

(b) Axial station, 14 inches.

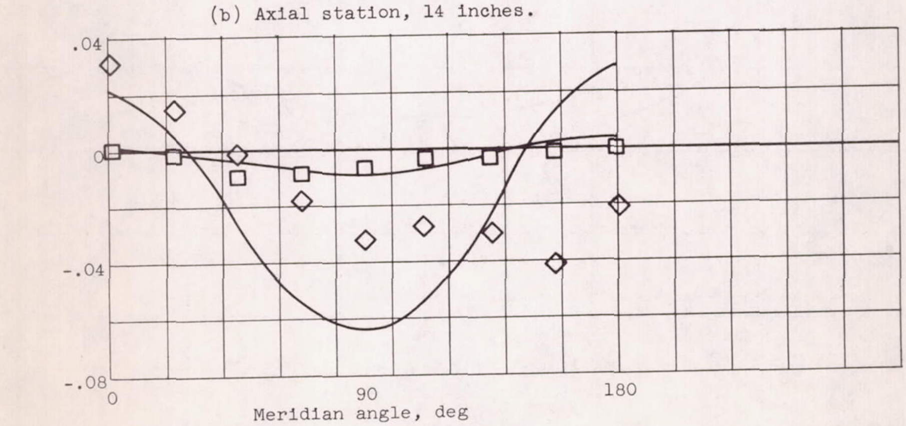

(c) Axial station, 20.5 inches.

Figure 7. - Effect of crossflow separation on agreement between theory and experiment for model 2 at Reynolds number of 14×10^6.

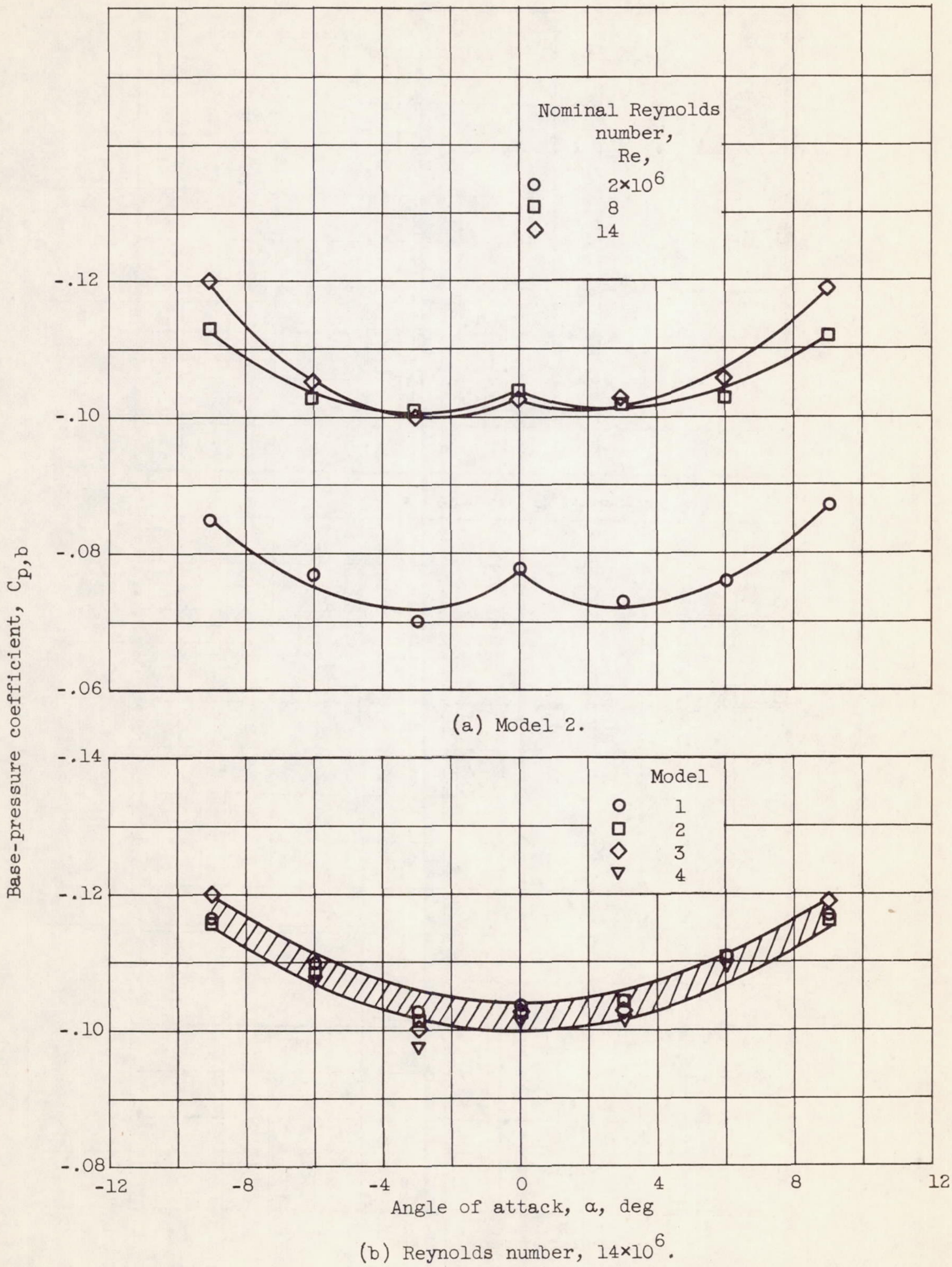

Figure 8. - Variation of base-pressure coefficient with Reynolds number and nose-fineness ratio.

3036

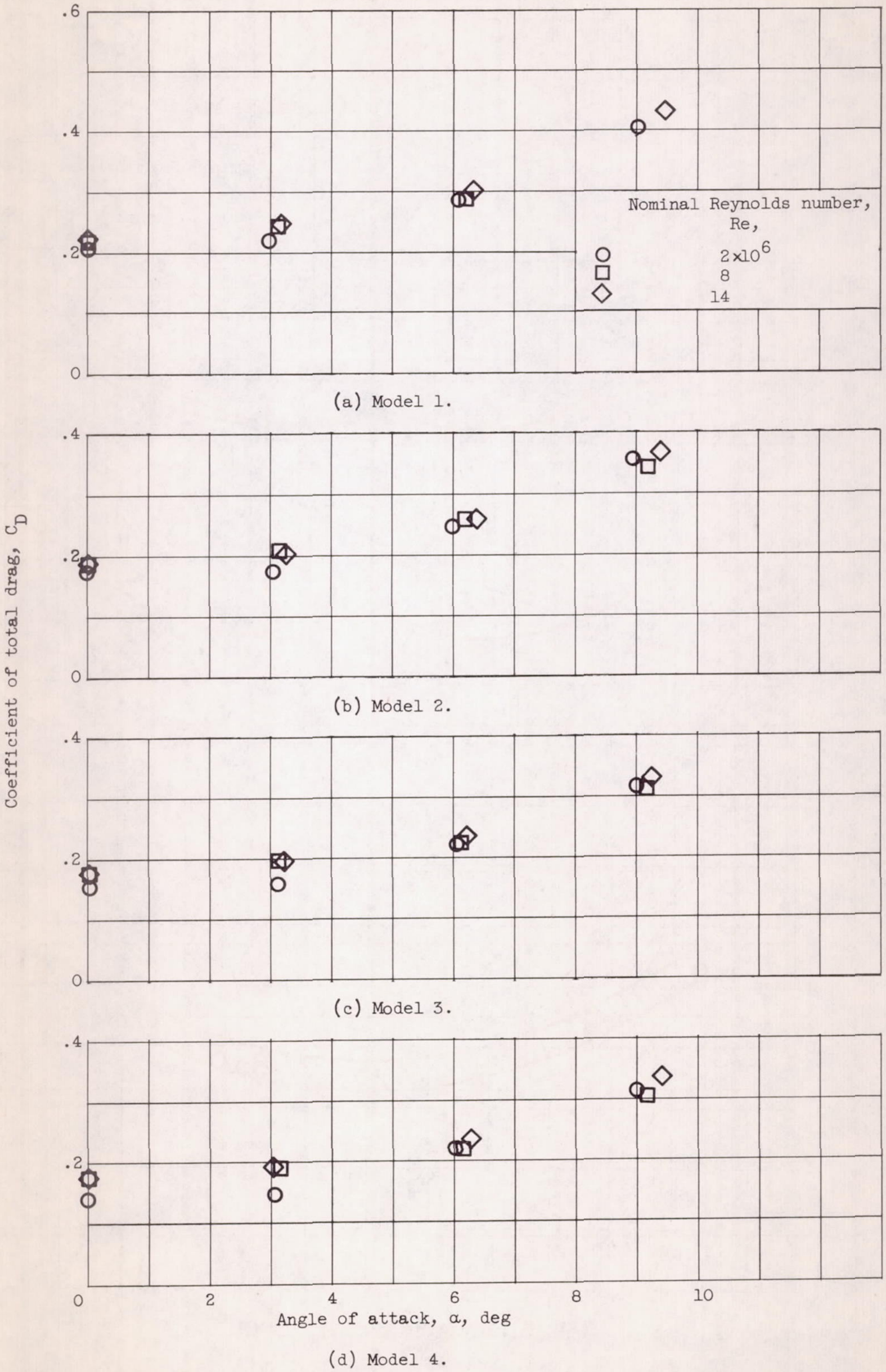

Figure 9. - Variation of total-drag coefficient with angle of attack for all models.

3036

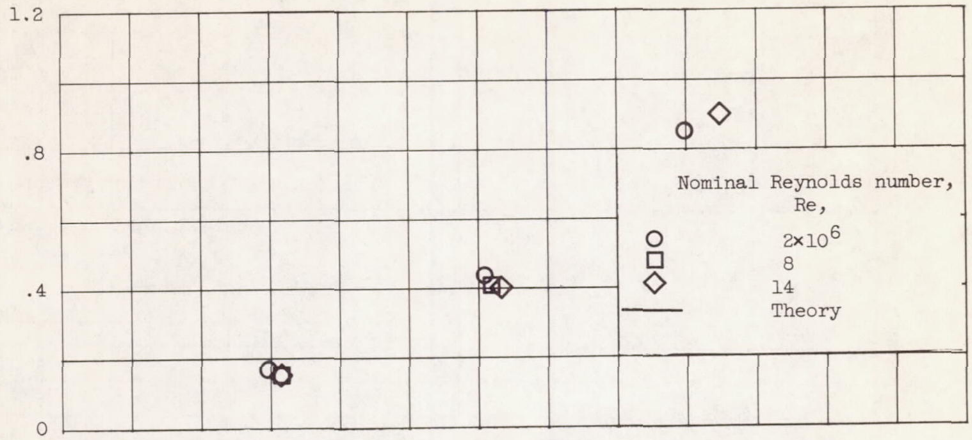

(a) Model 1.

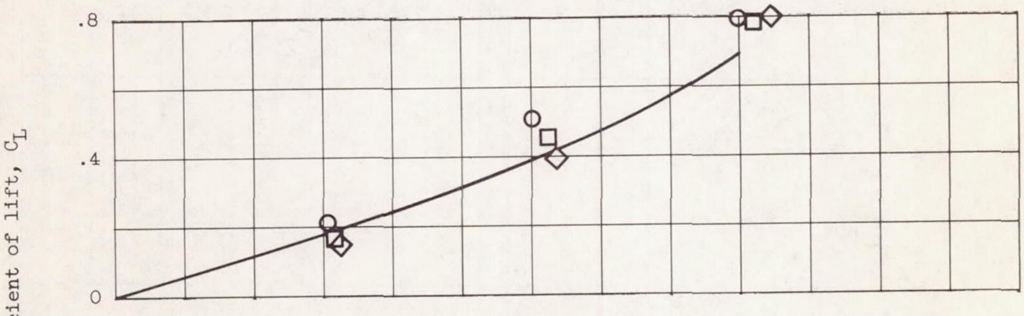

(b) Model 2.

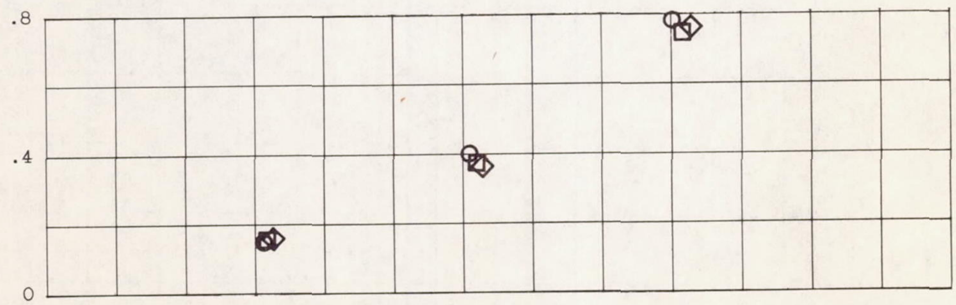

(c) Model 3.

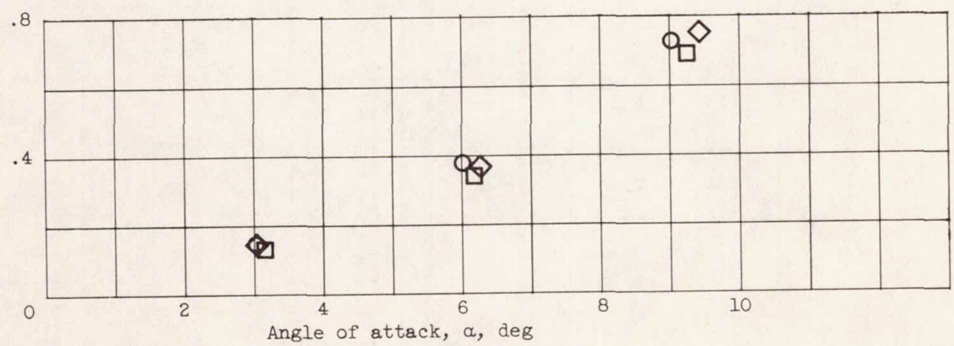

(d) Model 4.

Figure 10. - Variation of lift coefficient with angle of attack for all models.

3036

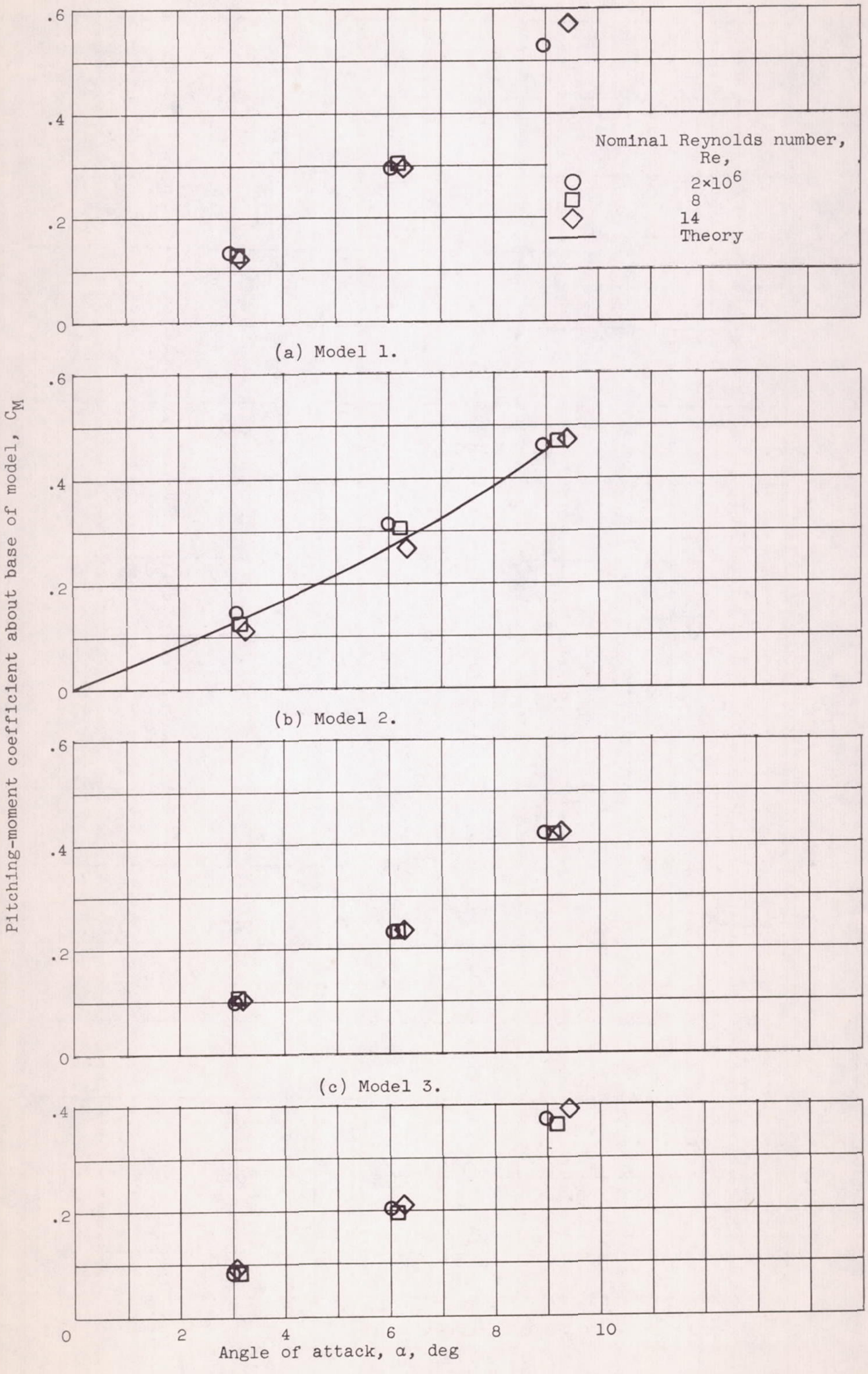

Figure 11. - Variation of pitching-moment coefficient with angle of attack for all models.

3036

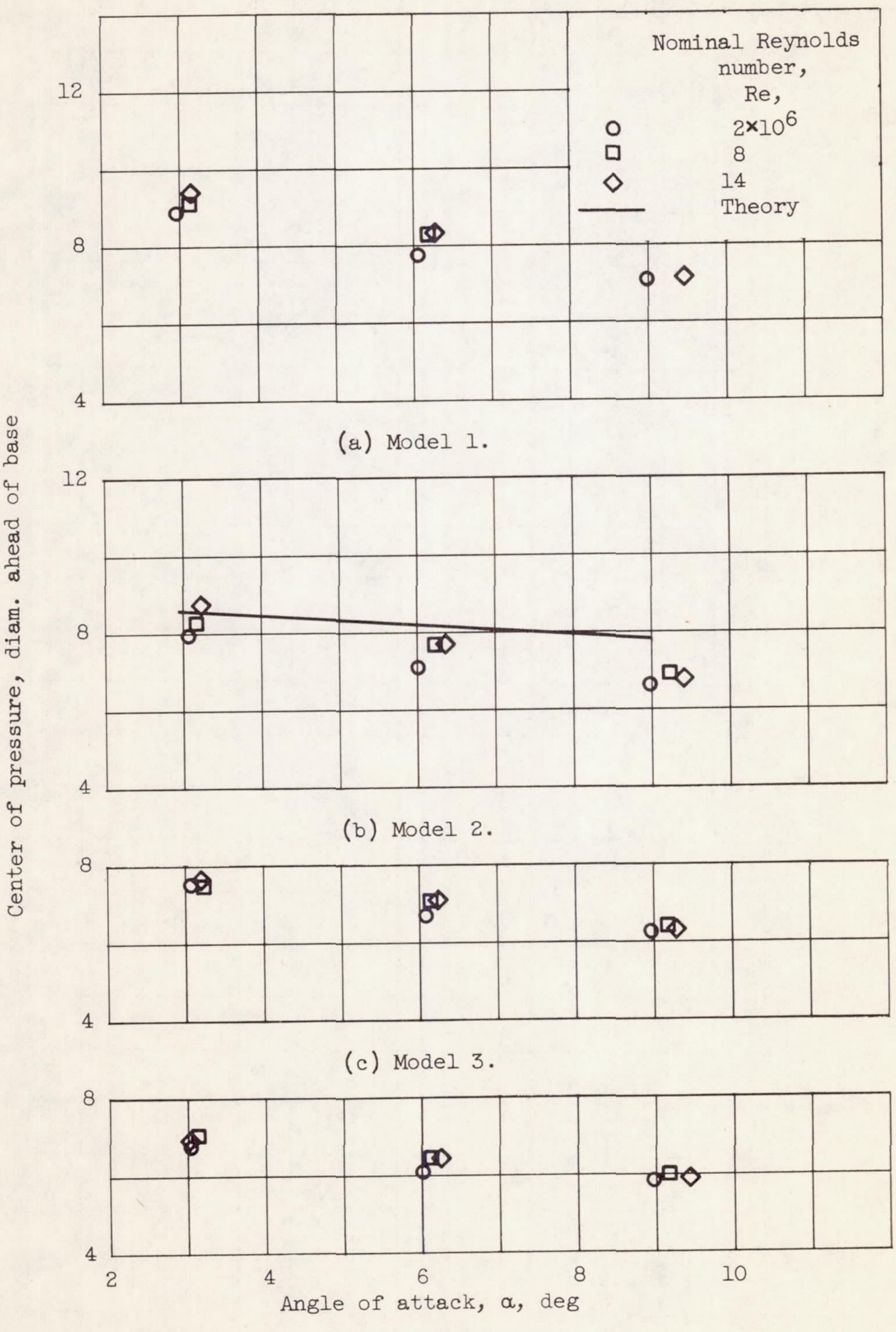

(a) Model 1.

(b) Model 2.

(c) Model 3.

(d) Model 4.

Figure 12. - Variation of center of pressure with angle of attack for all models.

3036

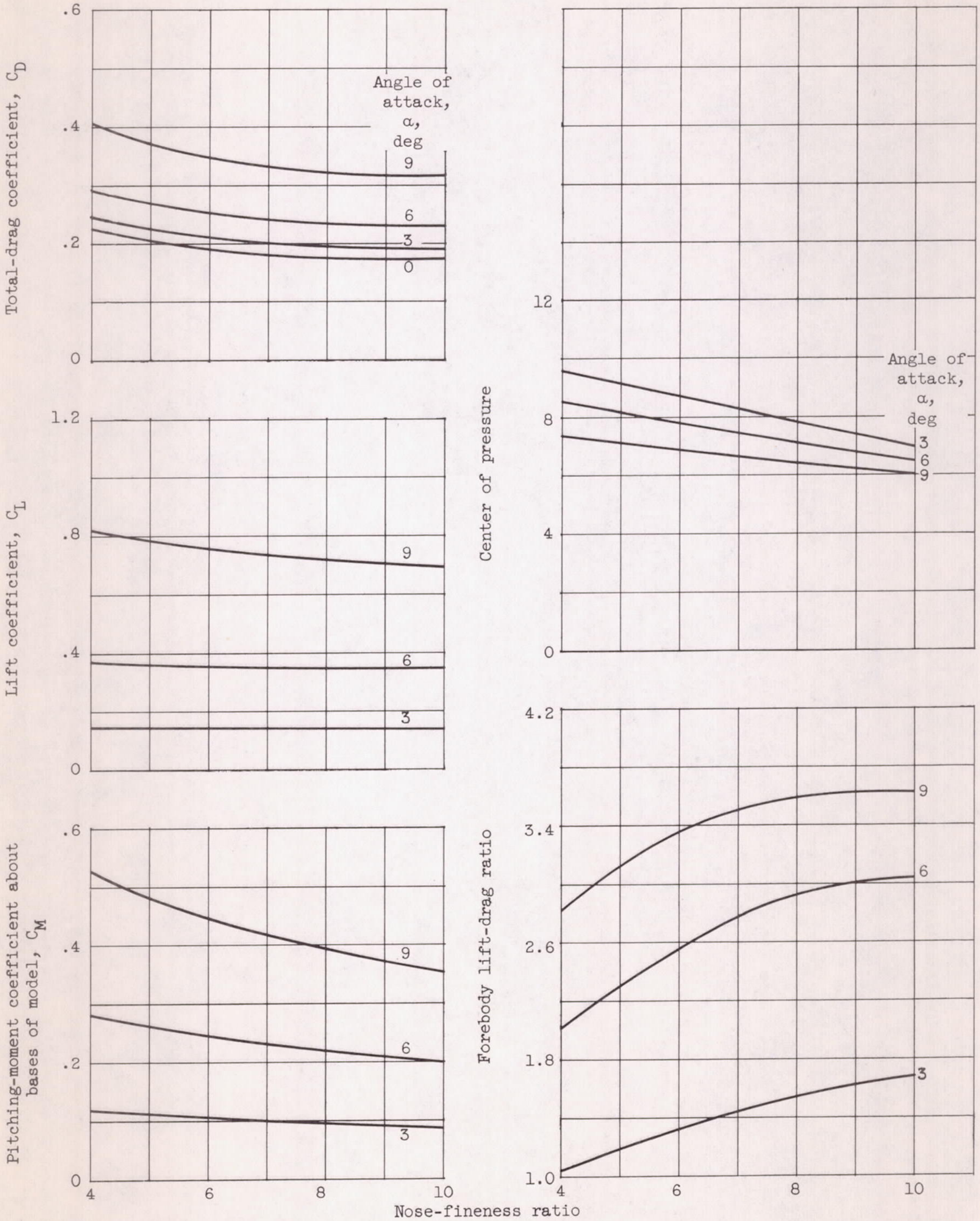

Figure 13. - Variation of force parameters with nose-fineness ratio at Reynolds number of 14×10^6.

NACA-Langley - 1-25-54 - 325